
3 Calcium Signaling in Dendritic Spines

William R. Holmes

CONTENTS

3.1	Introduction	26
3.2	First-Generation Dendritic-Spine Calcium Models	27
3.2.1	Calcium Diffusion	27
3.2.2	Calcium Buffering	28
3.2.3	Calcium Pumps	29
3.2.4	Calcium Influx	29
3.2.5	Calcium from Intracellular Stores	30
3.2.6	Summary	30
3.3	Insights from First-Generation Dendritic-Spine Calcium Models	31
3.3.1	Spines Compartmentalize Calcium Concentration Changes	31
3.3.2	Spines Amplify Calcium Concentration Changes	31
3.3.3	Spine-Head Calcium (or CaMCA ₄) Concentration is a Good Predictor of LTP ...	31
3.3.4	Spine Shape Plays an Important Role in the Ability of a Spine to Concentrate Calcium	32
3.4	Issues with Interpretation of First-Generation Spine-Calcium Model Results	32
3.4.1	Calcium Pumps	32
3.4.2	Calcium Buffers	33
3.4.3	Calcium Source	34
3.5	Imaging Studies Test Model Predictions	34
3.5.1	Spines Compartmentalize Calcium Concentration Changes	34
3.5.2	Importance of Spine Geometry	35
3.6	Insights into Calcium Dynamics in Spines from Experimental Studies	35
3.6.1	Sources of Calcium in Spines	36
3.6.1.1	NMDA-Receptor Channels	36
3.6.1.2	Voltage-Gated Calcium Channels	36
3.6.1.3	Calcium Stores	37
3.6.1.4	Implications for Models	38
3.6.2	Calcium Extrusion via Pumps	38
3.6.3	Calcium Buffers in Spines	38
3.7	Additional Insights into Spine Function from Experimental Studies	39
3.7.1	Spine Motility	39
3.7.2	Coincidence Detection with Backpropagating Action Potentials	40
3.8	Second-Generation Spine Models: Reactions Leading to CaMKII Activation	40
3.8.1	Modeling CaMKII Activation is Complicated	41
3.8.2	Characteristics of Second-Generation Models	41
3.8.2.1	Deterministic vs. Stochastic	42
3.8.2.2	Calcium Signal	43

3.8.2.3	Calcium Binding to Calmodulin	43
3.8.2.4	CaMKII Autophosphorylation Reactions	43
3.8.2.5	CaMKII Dephosphorylation Reactions	46
3.8.2.6	Other Reactions	47
3.9	Insights from Second-Generation Models	48
3.9.1	Frequency Dependence of CaMKII Activation	48
3.9.2	Different Stages of CaMKII Activation	48
3.9.3	CaMKII Activation as a Bistable Molecular Switch	49
3.9.4	CaMKII and Bidirectional Plasticity	50
3.9.5	CaMKII Activation and Spine Shape	50
3.9.6	Models Predict the Need for Repetition of Short Tetanus Trains	51
3.10	Future Perspectives	51
3.11	Summary	53
	Appendix 1. Translating Biochemical Reaction Equations to Differential Equations	55
	Appendix 2. Stochastic Rate Transitions	56
	Appendix 3. Use of Michaelis–Menten Kinetics in Dephosphorylation Reactions	57

3.1 INTRODUCTION

The function of dendritic spines has been debated ever since they were discovered by Ramón y Cajal in 1891. Although it was widely believed that spines were important for intercellular communication, the small size of dendritic spines prevented confirmation of this function until 1959, when Gray, using the electron microscope, showed that synapses are present on spines. We now know that in many cell types the vast majority of excitatory synapses are on spines rather than on dendrites. Why should excitatory synapses be on spines rather than on dendrites? What role does spine morphology play in their function? Because spines are so small, with surface area generally less than $1 \mu\text{m}^2$, these questions have been difficult to address experimentally. Up until about ten years ago, leading ideas about the function of spines were based on mathematical models and computer simulations. However, in recent years, the development of sophisticated imaging techniques, particularly two-photon microscopy, has allowed questions about spine function to be addressed experimentally (Denk et al., 1996).

Early theoretical studies of passive spines focused on the electrical resistance provided by the thin spine stem, R_{SS} , and suggested that changes in spine-stem (neck) diameter might be important for synaptic plasticity (Rall, 1974, 1978). Specifically, if the ratio of the spine-stem resistance to the input resistance at the dendrite at the base of the spine (R_{SS}/R_{BI}) was between 0.1 and 10 (or considering synaptic conductance, g_{syn} , between 0.1 and 10 times $[1 + 1/(g_{syn}R_{BI})]$), then a small change in spine-stem diameter could have a significant effect on the voltage in the dendrite due to input at the spine head. Later theoretical studies in the 1980s and early 1990s (reviewed by Segev and Rall, 1998) proposed that if spines possessed voltage-gated ion channels, then interactions among excitable spines could amplify synaptic input and create a number of additional interesting computational possibilities for information transfer. However, both the earlier passive and later active spine theoretical studies required R_{SS} to be 200 to 2000 $\text{M}\Omega$ for their most interesting predictions to occur. Unfortunately, when it finally became possible to estimate R_{SS} with imaging techniques in the mid-1990s, it was found that R_{SS} was 5 to 150 $\text{M}\Omega$ in many neuron types (Svoboda et al., 1996). The latest models of excitable spines reduced the required R_{SS} value to 95 $\text{M}\Omega$ by assuming kinetics for a low-threshold calcium conductance in the spine head, but low-threshold T-type calcium channels most probably do not exist on spines in the densities required by these models (Sabatini and Svoboda, 2000).

While the theoretical studies described above searched for a function for spines that depended on the *electrical* resistance of the spine neck, the spine neck might also provide a *diffusional* resistance

to the flow of ions and molecules. Koch and Zador (1993) refer to the spine neck as having a small *diffusive space constant*. By restricting the flow of materials out of the spine head, the spine neck might effectively isolate the spine head and provide a localized environment where reactions specific to a particular synapse can occur. Calcium is a prime candidate for a substance that might be selectively concentrated in the spine head. Calcium is important for a large number of metabolic processes and has been shown necessary for the induction of long-term potentiation (LTP), but high concentrations of calcium can lead to cell death. Spines might provide isolated locations where high concentrations of calcium could be attained safely without disrupting other aspects of cell function (Segal, 1995). In this chapter we review theoretical models and experimental evidence suggesting that a major function of dendritic spines is to concentrate calcium. We discuss factors affecting calcium dynamics in spines and subsequent calcium-initiated reaction cascades, focusing on spines in hippocampal CA1 pyramidal cells. We do this from the point of view of developing realistic computational models to gain insights into these processes.

3.2 FIRST-GENERATION DENDRITIC-SPINE CALCIUM MODELS

First-generation dendritic-spine calcium models were developed because studies had shown that calcium was necessary for the induction of LTP (Wigstrom et al., 1979; Turner et al., 1982; Lynch et al., 1983). LTP induction requires a strong, high-frequency tetanus; a weak stimulus delivered at low to moderate frequencies can be applied as often as desired without producing potentiation. These frequency and cooperativity requirements of LTP must produce a steep nonlinearity to enable potentiation to occur. The hypothesis behind first-generation models was that there should be a steep nonlinearity in spine-head calcium concentration as a function of the number of activated synapses and the frequency of activation. Any nonlinearity in spine-head calcium concentration could be amplified further by subsequent calcium-initiated reactions.

The first-generation models, although sharing many similarities, can be divided into three groups based on the method of calcium entry into the spine head. Models by Gamble and Koch (1987) and Wickens (1988) assumed that calcium enters via voltage-dependent calcium channels. The models by Holmes and Levy (1990) and Zador et al. (1990) had calcium entering through NMDA-receptor channels, while Schiegg et al. (1995) also included calcium release from intracellular stores. Some variant of these models forms the basis of most spine models in use today. These spine models are coupled, either directly or indirectly, with a model of a cell that, for a specified input condition, calculates voltage at the spine head as a function of time. This enables calcium influx through voltage-gated calcium channels and NMDA-receptor channels to be computed appropriately.

3.2.1 Calcium Diffusion

The starting point for modeling calcium diffusion in dendritic spines is the one-dimensional diffusion equation, $\partial C/\partial t = D\partial^2 C/\partial x^2$, also called Fick's second law of diffusion. Dendritic-spine models use a discretized form of this equation in which spine geometry is represented as a series of cylindrical compartments with one or more compartments for the spine head, one or more compartments for the spine neck, and one or more compartments for the dendritic shaft. Examples are shown in Figure 3.1. It is assumed that calcium is "well-mixed" within each compartment with calcium concentration varying only between compartments. The change in calcium concentration in compartment i due to diffusion is represented mathematically as

$$\left. \frac{d[\text{Ca}]_i}{dt} \right|_{\text{diffusion}} = -\frac{D}{V_i} \left\{ \left(\frac{A}{\delta} \right)_{i,i-1} ([\text{Ca}]_i - [\text{Ca}]_{i-1}) + \left(\frac{A}{\delta} \right)_{i,i+1} ([\text{Ca}]_i - [\text{Ca}]_{i+1}) \right\}, \quad (3.1)$$

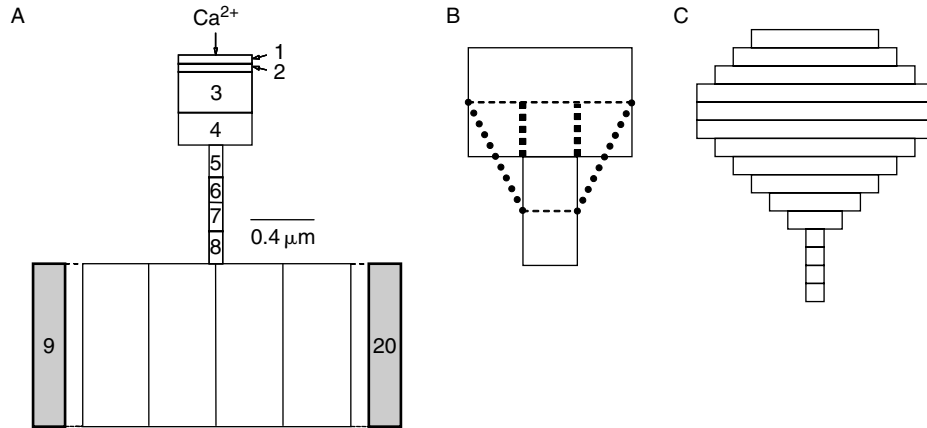


FIGURE 3.1 Compartmental representations of a spine. (A) A typical representation. (B) The boundary condition between the spine head and the spine neck can be modeled as being smooth or abrupt. Smooth coupling uses Equation (3.2) with the actual cross-sectional areas of the compartments bordering the head–neck boundary (angled heavy dotted lines). Abrupt coupling uses the neck cross-sectional area for both the neck and head compartments (vertical heavy dotted lines). (C) A representation with variable spine-head diameter.

where $[Ca]_i$ is the concentration of free calcium in compartment i , D is the calcium diffusion coefficient, V_i is the volume of the i th compartment, and $(A/\delta)_{i,j}$ is the coupling coefficient between compartments i and j .

This coupling term can be defined in two different ways depending on whether the transition between compartments of unequal diameter is assumed to be smooth or abrupt. For smooth coupling, the coupling coefficient is defined as

$$\left(\frac{A}{\delta}\right)_{i,j} = 2 \left(\frac{A_i \delta_i + A_j \delta_j}{(\delta_i + \delta_j)^2} \right), \quad (3.2)$$

where A_i and A_j are the cross-sectional areas and δ_i and δ_j are the thicknesses (or lengths) of compartments i and j , respectively. Abrupt coupling can be expressed with the same equation except that A_i and A_j are assumed to be equal to the cross-sectional area of the smaller compartment, typically the spine neck. Only calcium in the spine head just above the spine-neck opening is allowed to diffuse into the spine neck. The distinction is illustrated in Figure 3.1. Note, Equation (3.2) reduces to A_i/δ_i when the compartments are identical in size and to $1/\delta_i^2$ when divided by the volume, V_i .

In practice, the distinction between smooth and abrupt coupling matters little except at the transitions between spine head and neck and between spine neck and dendrite when the number of compartments is small. At these transitions one must choose compartment number and size carefully to ensure that spine shape is represented appropriately. Spine-head calcium concentration will decay significantly faster with smooth coupling and a coarse grid than with either abrupt coupling or smooth coupling with a fine grid. The use of a fine grid with abrupt coupling (as in Figure 3.1C) may be the simplest way to match specific spine morphology most accurately.

3.2.2 Calcium Buffering

Once calcium enters the cell it binds to buffers. Spines are known to possess a number of calcium-binding proteins, such as calmodulin, calcineurin, and calbindin, as well as immobile buffers and calcium stores. First-generation spine calcium models considered simple 1:1 buffering to an unspecified buffer or, in some cases, 4:1 buffering of calcium by calmodulin with buffer concentration

being fixed within each compartment. Consequently, the change in calcium concentration due to buffering was modeled as

$$\left. \frac{d[\text{Ca}]_i}{dt} \right|_{\text{buffer}} = \sum_j -k_{f_j} [\text{Ca}]_i [B_j]_i + k_{b_j} ([B_{t_j}]_i - [B_j]_i), \quad (3.3)$$

where k_{f_j} and k_{b_j} are the forward and backward rate constants for binding of calcium to buffer for buffer j and $[B_j]_i$ and $[B_{t_j}]_i$ are the free concentration and total concentration (bound plus unbound) of buffer j in compartment i . Equations are also required for free-buffer concentration,

$$\frac{d[B_j]_i}{dt} = -k_{f_j} [\text{Ca}]_i [B_j]_i + k_{b_j} ([B_{t_j}]_i - [B_j]_i), \quad (3.4)$$

for each buffer j in each compartment i .

3.2.3 Calcium Pumps

There are a number of calcium pumps thought to be present in spines, including a high-affinity, low-capacity ATP-dependent pump, a low-affinity, high-capacity $\text{Na}^+ - \text{Ca}^{2+}$ exchanger, and a SERCA pump that pumps calcium into intracellular stores. These pumps are modeled either as first-order processes

$$\left. \frac{d[\text{Ca}]_i}{dt} \right|_{\text{pump}} = \sum_j -k_{p_j} \frac{A_i}{V_i} ([\text{Ca}]_i - [\text{Ca}]_r), \quad (3.5)$$

where k_{p_j} , the pump velocity for pump j , is multiplied by the surface-to-volume ratio for compartment i and $[\text{Ca}]_r$ is the resting calcium concentration, or as Michaelis–Menten processes

$$\left. \frac{d[\text{Ca}]_i}{dt} \right|_{\text{pump}} = \sum_j -k_{m_j} P_{\max_j} \frac{A_i}{V_i} \frac{[\text{Ca}]}{[\text{Ca}] + K_{d_j}} + \frac{A_i}{V_i} J_{\text{leak}}, \quad (3.6)$$

where k_{m_j} is the maximum turnover rate for pump j , P_{\max_j} is the surface density of pump sites for pump j (the product $k_m P_{\max}$ is a measure of pump efficiency), K_{d_j} is the dissociation constant for pump j (a measure of pump affinity for calcium), and J_{leak} is the leak flux needed to maintain calcium concentration at its resting value.

3.2.4 Calcium Influx

As previously noted, first-generation spine models used different sources of calcium for calcium influx into spines. When the source of calcium is voltage-dependent calcium channels, the computation for calcium influx is straightforward. Calcium current at the spine head is computed in the neuron-level model and this current is converted into moles of calcium ions entering the volume of the most distal spine-head compartment per time interval (Gamble and Koch, 1987; Wickens, 1988). However, computation of calcium influx through NMDA-receptor channels is complicated by the fact that this current is a mixed Na/K/Ca current. Fortunately, the relative permeabilities of NMDA-receptor channels for Na, K, and Ca have been determined (Mayer and Westbrook, 1987) and computations with the constant-field equations can determine the calcium component of the NMDA-receptor channel current at a given voltage. Perhaps not surprisingly, the calcium proportion of the current through NMDA-receptor channels is relatively constant, being 8% to 12% over the physiological range of voltages. Zador et al. (1990) assumed a fixed 2% of the NMDA current was

calcium, while Holmes and Levy (1990) used constant-field equation calculations to determine the calcium component.

3.2.5 Calcium from Intracellular Stores

Schiegg et al. (1995) extended the dendritic-spine model to include calcium release from internal stores. There are a number of ways in which release from stores can be modeled. Following the model of Schiegg et al. (1995), release from stores in compartment i is modeled as

$$\left. \frac{d[\text{Ca}]_i}{dt} \right|_{\text{stores}} = \rho X ([\text{Ca}_{\text{store}}]_i - [\text{Ca}]_i), \quad (3.7)$$

where ρ is the store depletion rate, X is the fraction of open channels, and $[\text{Ca}_{\text{store}}]_i$ is the store calcium concentration in compartment i . Store calcium concentration is modeled by

$$\frac{d[\text{Ca}_{\text{store}}]_i}{dt} = -\rho X ([\text{Ca}_{\text{store}}]_i), \quad (3.8)$$

where store refilling is ignored for the short time course of the simulations (although refilling could be added with a term similar to the right-hand sides of Equations [3.5] or [3.6] being added to Equation [3.8]). Schiegg et al. (1995) limit the stores to one compartment within the spine head. The fraction of open channels, X , is described by

$$\frac{dX}{dt} = -\frac{1}{\tau_{\text{store}}} (X - (RA)\text{Re}(\text{Ca}_i)), \quad (3.9)$$

where τ_{store} is the time constant for channel closing, RA is the probability of agonist binding to IP₃ (inositol triphosphate) or ryanodine receptors (RA is assumed to be either 0, no agonist available, or 1, saturating concentration of agonist, in the simulations), and $\text{Re}(\text{Ca}_i)$ expresses the calcium dependence of calcium release. $\text{Re}(\text{Ca}_i)$ is defined for $[\text{Ca}]_i$ greater than $[\text{Ca}]_\theta$ by

$$\text{Re}(\text{Ca}_i) = R_0 \frac{([\text{Ca}]_i - [\text{Ca}]_\theta)}{([\text{Ca}]_{\text{max}} - [\text{Ca}]_\theta)} \exp\left(-\frac{([\text{Ca}]_i - [\text{Ca}]_\theta)}{([\text{Ca}]_{\text{max}} - [\text{Ca}]_\theta)}\right), \quad (3.10)$$

where $[\text{Ca}]_\theta$ is the threshold for calcium release and $[\text{Ca}]_{\text{max}}$ is the calcium concentration where the maximum release occurs. This release function is an alpha function with normalizing constant R_0 . Although calcium release from stores is thought to have a bell-shaped dependence on calcium concentration, the use of an alpha function allows release via IP₃-receptor activation and ryanodine-receptor activation to be modeled with one function. This is done purely for convenience.

3.2.6 Summary

In the preceding sections, we have given various components of the differential equation for the change in calcium concentration in a spine-head compartment. All of these components must be combined into a single differential equation for the change of calcium concentration. That is,

$$\frac{d[\text{Ca}]_i}{dt} = \left. \frac{d[\text{Ca}]_i}{dt} \right|_{\text{diffusion}} + \left. \frac{d[\text{Ca}]_i}{dt} \right|_{\text{buffer}} + \left. \frac{d[\text{Ca}]_i}{dt} \right|_{\text{pump}} + \left. \frac{d[\text{Ca}]_i}{dt} \right|_{\text{stores}} + \text{influx}_i, \quad (3.11)$$

where the components due to diffusion, buffer, pumps, and stores are given by Equations (3.1), (3.3), (3.5) or (3.6), and (3.7), respectively. The influx term should be calculated in a neuron-level model, but often it is assumed to follow some simple functional form. Typically, only the outermost

spine-head compartment receives calcium influx. For each compartment in the spine-head model, it will be necessary to solve Equation (3.11) for calcium concentration and Equations (3.4) and (3.8) for buffer and calcium-store concentration along with the auxiliary calcium-store equations, Equations (3.9) and (3.10). For the 20-compartment spine model shown in Figure 3.1, the system would have 100 equations, 20 each for calcium concentration, buffer concentration, and calcium-store calcium concentration, plus 40 auxiliary equations for calcium stores.

3.3 INSIGHTS FROM FIRST-GENERATION DENDRITIC-SPINE CALCIUM MODELS

The goal of first-generation spine-calcium models was to see whether stimulation conditions that induce LTP could create large, nonlinear increases in spine-head calcium concentration as a function of frequency and strength of the stimulus. These models found this nonlinearity and produced a number of other insights and predictions.

3.3.1 Spines Compartmentalize Calcium Concentration Changes

A brief high-frequency train of input was found to cause calcium concentration changes in the spine that were restricted to the spine head. Gamble and Koch (1987) found that spine-head calcium concentration could reach micromolar concentrations after seven spikes in 20 msec due to influx through voltage-dependent calcium channels. Holmes and Levy (1990), using eight pulses at 400 Hz, and Zador et al. (1990), using three pulses at 100 Hz paired with depolarization to -40 mV, found that calcium influx through NMDA-receptor channels could increase spine-head calcium concentration to $10 \mu\text{M}$ or more. In each of these models, the calcium transient was restricted to the spine head with very little calcium making its way through the spine neck to the dendrite. Zador et al. (1990) modeled calcium binding to calmodulin and found that compartmentalization of calmodulin fully loaded with calcium ions (CaMCa_4) was even more pronounced.

3.3.2 Spines Amplify Calcium Concentration Changes

When the same input stimulus that caused spine-head calcium to rise to over $10 \mu\text{M}$ was placed on the dendrite instead of the spine head, the local calcium concentration change was 1 to 2 orders of magnitude smaller. The magnitude of this difference depended on spine shape (Holmes, 1990; Zador et al., 1990). Large calcium concentrations were possible in the spine head because of its small volume and the restricted diffusion out of the spine head caused by the thin spine neck.

What was surprising was not so much that spines amplify calcium concentration changes compared to dendrites, but how few NMDA channels are needed to produce significant amplification. The NMDA conductance plots in Holmes and Levy (1990) indicate that the amplification occurred despite the average number of open NMDA-receptor channels during tetanic stimulation being much less than one (because of voltage-dependent magnesium block). This is consistent with numbers recently reported by Nimchinsky et al. (2004). Zador et al. (1990) obtained large amplification in their model assuming that the calcium component of the NMDA current was only 2% of the total, or about fivefold less than current estimates. These models found it all too easy to predict that spine-head calcium changes should be huge, even with small numbers of NMDA receptors at the synapse.

3.3.3 Spine-Head Calcium (or CaMCa_4) Concentration is a Good Predictor of LTP

Holmes and Levy (1990) and Zador et al. (1990) modeled spine-head calcium (or CaMCa_4) concentration as a function of input frequency and intensity and found that peak spine-head calcium

concentration showed the same nonlinear dependence on input frequency and intensity as LTP. The results provided support for Lisman's theory (Lisman, 1989) that low to moderate levels of spine-head calcium concentration produce LTD and high levels produce LTP.

Peak spine-head calcium levels in the model were also correlated with the finding of LTP or no LTP in the relative timing of weak and strong inputs in the experiment of Levy and Steward (1983), an experimental result that foreshadowed the recent excitement about spike timing dependent plasticity (STDP). In that experiment, a weak contralateral tetanic input (eight pulse 400 Hz) was delivered just before or just after a strong ipsilateral tetanus. LTP was observed in the weak pathway if the weak input was delivered 1, 8, or 20 msec before the strong input, but LTD occurred if the weak input came after the strong input. The Holmes and Levy (1990) model found that spine-head calcium concentration was high when the weak input came before the strong input, but was low with the reverse pairing.

3.3.4 Spine Shape Plays an Important Role in the Ability of a Spine to Concentrate Calcium

While most early models assumed a spine shape resembling that of a long-thin spine, Holmes (1990) and Gold and Bear (1994) compared calcium concentration changes in long-thin, mushroom-shaped, and stubby spines. Spine dimensions for these categories of spines were taken from a study of dentate granule cells by Desmond and Levy (1985). While calcium concentration in the long-thin spine reached 28 μM in the models, levels in mushroom-shaped and stubby spines peaked at less than 2 μM . Although peak concentration was about the same in the mushroom-shaped and stubby spines, the calcium transient decayed faster in the stubby spine as calcium did not face a spine-neck diffusion barrier and rapidly diffused into the dendrite.

The quantitative numbers from these two studies can be criticized on several grounds. First, the huge change in the long-thin spine occurred when the fast buffer became saturated, while the larger spine-head volume and more buffer sites prevented buffer saturation in mushroom-shaped and stubby spines. The issue of appropriate buffer kinetics and concentrations will be discussed further in Section 3.4. Second, the input was identical for the different-shaped spines, but the larger mushroom-shaped and stubby spines are likely to have larger postsynaptic densities and hence, more NMDA receptors and more calcium influx. Nevertheless, more recent models with a slower, nonsaturating buffer and an input dependent on spine-head size also show that spine-head calcium levels are strongly dependent on spine shape. However, the differences between levels attained in long-thin and mushroom shaped spines are 2 to 5-fold rather than the 18-fold reported by the studies mentioned above.

3.4 ISSUES WITH INTERPRETATION OF FIRST-GENERATION SPINE-CALCIUM MODEL RESULTS

The major problem with interpreting results from first-generation spine-calcium models is that values for many key parameters used in these models are not known in general and are not known for dendritic spines in particular. Parameter values used in the equations given above are summarized in Table 3.1.

3.4.1 Calcium Pumps

The densities, kinetics, pump velocity, and turnover rates for the various types of pumps that may exist on spines are not known. In the models, the pump parameters have a quantitative effect on results, but not a qualitative one. The pumps reduce the peak spine-head calcium concentration only a little, but do play a significant role in the final calcium decay rate. Zador et al. (1990) proposed that pumps on the spine neck might isolate the spine head from calcium concentration changes in the dendrites.

TABLE 3.1
Parameter Values for First-Generation Dendritic-Spine Models

	Description	Value	Model	Equation
D_{Ca}	Calcium diffusion coefficient	$0.6 \mu\text{m}^2 \text{msec}^{-1}$	Holmes, Zador, Schiegg	3.1
k_p	Pump rate constant	$1.4 \times 10^{-4} \text{cm sec}^{-1}$	Holmes	3.5
k_{bf}	Forward buffer rate constant (calmodulin)	$0.5 \mu\text{M}^{-1} \text{msec}^{-1}$ $0.05 \mu\text{M}^{-1} \text{msec}^{-1}$ $0.5 \mu\text{M}^{-1} \text{msec}^{-1}$	Holmes Zador Schiegg	3.3 and 3.4
k_{bb}	Backward buffer rate constant (calmodulin)	0.5msec^{-1} 0.5msec^{-1} 0.5msec^{-1}	Holmes Zador Schiegg	3.3 and 3.4
B_t	Total buffer concentration	200/100 μM 100 μM 120 μM	Holmes Zador Schiegg	3.3 and 3.4
k_m	Maximum pump turnover rate	0.2msec^{-1}	Zador	3.6
$k_m P_{\text{max}}$	Pump efficiency (ATP-ase) Pump efficiency (Na/Ca exchanger)	$1 \times 10^{-15} \mu\text{mol msec}^{-1} \mu\text{m}^{-2}$ $5 \times 10^{-15} \mu\text{mol msec}^{-1} \mu\text{m}^{-2}$	Schiegg	3.6
K_d	Pump affinity (ATP-ase) Pump affinity (Na/Ca exchanger)	0.5 μM 20.0 μM	Zador, Schiegg	3.6
J_{leak}	Leak flux to balance pump at rest	$0.1 \times 10^{-15} \mu\text{mol msec}^{-1} \mu\text{m}^{-2}$ 1.25×10^{-17}	Schiegg	3.6
ρ	Store depletion rate	(150msec^{-1})	Schiegg	3.8
τ_{store}	Time constant for store channel closing	100 msec	Schiegg	3.9
RA	Probability of agonist binding to store receptor	0 or 1	Schiegg	3.9
R_0	Normalizing constant	$\exp(1)$	Schiegg	3.10
Ca_θ	Threshold for store Ca release	150 nM	Schiegg	3.10
Ca_{max}	Concentration where maximum release occurs	250 nM	Schiegg	3.10
Ca_{store}	Store Ca concentration Ca component of NMDA current	25 mM 2% 10% 8% to 12% computed	Schiegg Zador Schiegg Holmes	3.8
Ca_r	Resting Ca concentration	70 nM 50 nM 50 nM	Holmes Zador Schiegg	3.5

Pumps on the spine neck would be in an ideal position for this role since the surface-to-volume ratio would be very high in the spine neck for a given pump density.

3.4.2 Calcium Buffers

The numbers, types, mobilities, and concentrations of calcium buffers in dendritic spines are not known. A number of different assumptions have been made about calcium buffers in spines and these can have qualitative as well as quantitative consequences for models. If the buffer has fast kinetics and is saturable, as in Holmes and Levy (1990), small changes in buffer concentration

near the saturation point can have large quantitative effects on the level of spine-head calcium, as shown by Holmes (1990) and Gold and Bear (1994). Small changes in buffer concentration have less of a quantitative effect when buffer is not saturable or has low affinity or slow binding kinetics. Calmodulin, the major calcium buffer in Zador et al. (1990), is an example of a buffer with a relatively low calcium affinity, particularly for two of its four calcium-binding sites, and with calcium binding not being rapid. A difficulty with calmodulin as the primary buffer is that it is thought that only 5% of the approximately 40 μM calmodulin is free to bind calcium, at least in smooth-muscle cells (Luby-Phelps et al., 1995). A significant portion of the bound calmodulin may be released when calcium is elevated. If calmodulin is bound to neurogranin in the rest state and is released upon calcium influx (Gerendasy and Sutcliffe, 1997), then this added complication may not be a significant one.

While most model results suggest that spine-head calcium equilibrates quickly, some recent models have proposed that there is a calcium gradient within the spine head. Such a gradient cannot exist unless there is a very high concentration of fast immobile calcium buffer in the spine. Experimentally, it has been determined that equilibration of calcium in the spine head does occur and takes less than 2.5 msec (the time resolution of the optical scan) at room temperature (Majewska et al., 2000a). Because equilibration will be faster at physiological temperatures, it seems unlikely that spines have large concentrations of fast immobile buffer.

3.4.3 Calcium Source

While models consider calcium entering via voltage-gated channels or NMDA-receptor channels or from internal stores, no models to date incorporate all of these calcium sources. Holmes and Aradi (1998) modeled L, N, and T calcium channels on spine heads and found that the contribution of 5 N channels to calcium influx could be comparable to calcium influx through NMDA-receptor channels. But incorporation of all of these calcium sources poses another difficulty — calcium may rise too high in the model unless additional buffers or pumps are added.

3.5 IMAGING STUDIES TEST MODEL PREDICTIONS

The development and use of fluorescent calcium indicators with digital CCD camera imaging, confocal microscopy, and two-photon imaging has allowed spine calcium dynamics to be studied experimentally (Denk et al., 1996). Experimental studies have been able to test the predictions made by the models and have provided additional insights into calcium dynamics in spines and spine function.

3.5.1 Spines Compartmentalize Calcium Concentration Changes

Experiments by Muller and Connor (1991) using high-resolution fura-2 measurements suggested that spines could function as discrete compartments for calcium signaling. Svoboda et al. (1996) using two-photon imaging clearly showed that calcium can be compartmentalized in dendritic spines because of a diffusive resistance dependent on spine-neck length. What was more difficult to determine experimentally was the absolute amplitude and time course of the calcium transient in spines with different stimulation conditions. High-affinity indicators gave clear signals, but they tended to saturate at calcium concentrations above 1 μM . While low-affinity indicators could be used, the difficulty with any indicator is that the indicator itself acts as a calcium buffer, and calcium buffers, whether exogenous or endogenous, affect both the amplitude and time course of the transient (see discussion in Sabatini et al., 2001).

Despite these inherent difficulties, experimental estimates of peak spine-head calcium concentration have been made and these estimates have confirmed the predictions of the models.

Petrozzino et al. (1995) used a low-affinity indicator with CCD imaging and found that tetanic stimulation could raise spine-head calcium concentration to 20 to 40 μM . This increase in calcium was NMDA-receptor dependent, as it was blocked by APV. Yuste et al. (1999) paired five EPSPs with five action potentials and, taking into account the exogenous buffering by the indicator, estimated that calcium rose to 26 μM in the spine head (average of four spines). Sabatini et al. (2002), also taking into account buffering by the indicator, estimated that spine-head calcium reaches 12 μM for a single synaptic input when a magnesium block of NMDA receptors is relieved (by clamping to 0 mV). The extrapolation of this latter value to the physiological situation is difficult because voltage in cells is never “clamped” to 0 mV, the reversal potential for the NMDA current (although not for the calcium component of the current) is about 0 mV, and tetanic stimulation is likely to cause larger changes. Sabatini et al. (2002) also estimated the peak spine-head calcium concentration due to a single input at -70 mV to be 0.7 μM . NMDA-receptor channels are thought to be blocked at -70 mV so one would not expect any calcium influx, but it is not clear whether the voltage clamp was able to space clamp the voltage at the spine head being observed at this level.

3.5.2 Importance of Spine Geometry

Although experiments have not provided values for the peak of the spine-head calcium transient for different-shaped spines, the relative coupling between dendrite and spine has been compared for spines with different neck lengths. Volfovsky et al. (1999) used caffeine to stimulate calcium release from stores in spines with long, medium, and short neck lengths. They found that the amplitude of the spine-head calcium transient was not very different among spines with different shapes, but that the amplitude of the dendritic calcium transient was much closer in size to the spine-head transient for spines with short necks than for spines with long necks. In addition, the decay of the transient was faster in spines with short necks than in spines with long necks. The amplitudes of the spine-head transients in these experiments depended on the volume of caffeine-sensitive calcium stores in the different-shaped spines and thus depended on only one possible source of calcium influx into the spine. Majewska et al. (2000b) examined the diffusional coupling between spine and dendrite in the context of spine motility (motility is discussed further later). First they measured the calcium decay following a single action potential and found that spines with longer necks had slower decay kinetics than spines with shorter necks. Then they followed individual spines and measured changes in neck length and calcium decay at different time points over a 30-min period. They found that changes in neck length were correlated with changes in calcium decay. Holthoff et al. (2002) inferred calcium concentration changes in spines from fluorescence measurements following a backpropagating action potential. While they found a wide range of peak calcium concentration values in spines, they found no correlation between peak calcium and the diameter of the spine head suggesting that the density of calcium channels or stores compensates for changes in spine-head volume due to spine-head diameter. In agreement with the other two studies that are mentioned, they found that spines with longer necks had longer calcium decay times.

While these studies confirm the model prediction that calcium decay should be much shorter in stubby spines than in long-thin spines, the prediction about peak calcium concentration being much larger in long-thin spines than in stubby spines following synaptic or tetanic input remains to be tested.

3.6 INSIGHTS INTO CALCIUM DYNAMICS IN SPINES FROM EXPERIMENTAL STUDIES

Most of the problems with interpreting model results have to do with the fact that models have to make assumptions about unknown parameter values and processes. Whether the assumptions made are appropriate and realistic is often subject to debate. Recent experimental work has provided data that can be used to constrain model parameters and further refine spine calcium models. Insights from

recent work have been made regarding the sources of calcium in spines, the kinetics and importance of calcium pumps in spines, and the buffer capacity of spines in different cell types.

3.6.1 Sources of Calcium in Spines

The sources for calcium in spines are well-known. Calcium enters the spine cytoplasm through NMDA-receptor channels, voltage-gated calcium channels, and from internal calcium stores. (A small component may also enter through non-NMDA glutamate channels). However, the relative importance of each calcium source is a matter of controversy — a controversy that may have arisen from the study of different subsets of highly heterogeneous spine populations.

3.6.1.1 NMDA-Receptor Channels

NMDA-receptor channels provide the major source of calcium during synaptic input in CA1 hippocampal pyramidal cells (Yuste et al., 1999; Kovalchuk et al., 2000). How much calcium enters depends on the number of NMDA receptors at a synapse and whether NMDA receptors are saturated by a vesicle of glutamate. Both models and experiments predict that the number of NMDA receptors at a synapse is small (less than 20 for long-thin spines), but whether or not a quantum of glutamate, say 2000 molecules, will saturate this small number of receptors is not known. Total calcium influx will increase with each pulse in a high-frequency tetanus if NMDA receptors are not saturated, but will not increase if they are saturated. The most convincing evidence that NMDA receptors are not saturated by a single input was provided by Mainen et al. (1999) who showed that the calcium transient for a second input, delivered 10 msec after the first, was 80% as large as the calcium transient for the first input. Given that NMDA-receptor channels have a mean open time of about 10 msec and unbind glutamate slowly, these data suggest that glutamate clearance from the synaptic cleft must be fast, or at least fast compared to glutamate binding to NMDA receptors. As for models, the data provide constraints on the size and time course of calcium influx through NMDA-receptor channels for single inputs and tetanic input. In addition, they suggest that the synaptic current through NMDA receptors should be modeled stochastically. Recent models do this (Li and Holmes, 2000; Franks et al., 2001).

3.6.1.2 Voltage-Gated Calcium Channels

Cerebellar Purkinje cells do not have NMDA receptors, so voltage-gated calcium channels are likely to be the major calcium source in these cells. In CA1 pyramidal cells, voltage-gated calcium channels provide most of the calcium influx during backpropagating action potentials (Yuste et al., 1999). Unfortunately for modelers, calcium channels come in L-, N-, T-, P/Q-, and R-types with multiple subunit combinations and possible splice variants (e.g., Tottene et al., 2000; Pietroban, 2002). So the question is: How many calcium channels and what type(s) of voltage-gated calcium channels exist on spines?

Sabatini and Svoboda (2000) report that spines on CA1 pyramidal cells contain 1 to 20 calcium channels with the larger numbers found on spines with a larger volume. They report that these channels are predominantly R-type because blockers of L-, N-, and P/Q-types of calcium channels had no effect on spine calcium transients elicited by a backpropagating action potential. The involvement of T-type calcium channels could not be ruled out, but their experiments were done in a voltage range where T-type calcium channels were thought to be inactivated. They observed calcium transients in spines evoked by backpropagating action potentials that were larger or smaller than the dendritic transients — larger because of restricted diffusion out of the spine head and smaller because of failures of spine calcium channels to open. Yuste et al. (1999) used low concentrations of Ni^{2+} to selectively block low-threshold calcium currents and found that spine calcium transients elicited by backpropagating action potentials were not affected (this concentration of Ni^{2+} would also block some of the R-type calcium current as well — the G2 or R_a and R_b subtypes [Tottene et al., 2000]).

They concluded that CA1 pyramidal cell spines have high-threshold, but not low-threshold, calcium channels. Emptage et al. (1999) also used low concentrations of Ni^{2+} to rule out low-threshold calcium channel involvement in calcium transients during single synapse activation. Schiller et al. (1998) found that calcium influx in neocortical pyramidal cells was predominantly through N-, P/Q-, and T-type calcium channels, although they did not specifically rule out R- or L-types. They report that calcium-channel subtypes and densities in spines were similar to the subtypes and densities in the neighboring dendrite but were different in apical and basilar portions of the dendritic tree. These sets of data constrain the types of channels that need to be included in models, but perhaps more importantly, they indicate that spines are not sites of calcium “hot spots” and that calcium-channel densities in spines are much lower than densities needed to produce the interesting results in excitable spine models mentioned briefly at the beginning of this chapter.

3.6.1.3 Calcium Stores

How much calcium enters CA1 pyramidal spines from calcium stores compared to other sources is an area of controversy. Emptage et al. (1999) found that single afferent stimuli produced calcium transients in the spine head that were abolished by both NMDA and calcium induced calcium release (CICR) antagonists. They hypothesized that calcium entry through NMDA-receptor channels, although not large enough by itself to be detected reliably, is necessary to trigger calcium release from stores. Release from stores then provides the bulk of the calcium in the calcium transient. In contrast Kovalchuk et al. (2000) report that calcium transients in spines following weak subthreshold stimulation are primarily due to influx through NMDA-receptor channels. CICR antagonists ryanodine or CPA reduced the amplitude of the calcium signal by about 30%, leaving a large and easily detectable signal due to influx through NMDA-receptor channels. Surprisingly, blocking AMPA receptors with CNQX had little effect on the calcium transients, suggesting that voltage-dependent magnesium block of calcium influx through NMDA channels is incomplete near the resting potential (but see Yuste et al., 1999).

This controversy could be explained if the two studies were looking at different subsets of spines. Spacek and Harris (1997) report that only 58% of immature spines and 48% of adult spines have some form of a smooth endoplasmic reticulum (SER). The presence of an SER is much more prevalent in mushroom-shaped spines than in stubby or long-thin spines. Furthermore, the spine apparatus is found in more than 80% of mushroom-shaped spines but is rare in other spine types. If the SER and spine apparatus are the calcium stores in spines, as is believed, then one would expect to see CICR only in mushroom-shaped spines and in less than half of long-thin and stubby spines. The fact that Emptage et al. (1999) consistently observed CICR suggests that the spines they studied may have been predominantly mushroom-shaped spines. Emptage et al. (1999) also found that when CICR was blocked, repetitive stimulation was needed to bring calcium influx through NMDA-receptor channels up to the levels found with CICR. This is consistent with modeling study results mentioned earlier suggesting that mushroom-shaped spines have much smaller calcium transients than long-thin spines. Conversely, Kovalchuk et al. (2000) may have studied a larger proportion of spines lacking an SER. With CICR not being possible in most spines, influx through NMDA-receptor channels dominated the calcium transient. Regardless of whether or not stores play a role in spine calcium transients, a more important role for calcium stores in CA1 pyramidal cells may be in the generation of calcium waves that propagate down the thick apical shaft toward the soma (Nakamura et al., 2002).

In contrast to CA1 pyramidal cells, almost all Purkinje cell spines have an SER. Consequently, calcium stores are a major source of calcium in these cells. Finch and Augustine (1998) report that with repetitive stimulation (15 stimuli at 60 Hz) half of the calcium transient is due to IP_3 -mediated release from stores and half is due to calcium influx through voltage-gated calcium channels. The voltage-dependent influx, initiated by voltage changes produced by current through AMPA receptor channels, occurs first. IP_3 is produced following activation of metabotropic glutamate (mGlu) receptors, and induces a delayed calcium influx from stores.

3.6.1.4 Implications for Models

The experimental work elucidating the sources of calcium entry in spines has several implications for models. First, the numbers of NMDA receptors and voltage-dependent calcium channels at a spine are small and may require models to adapt a stochastic approach. Second, the number of NMDA receptors and calcium channels is correlated roughly with spine-head size. Although the type of calcium channel on spines, at least in CA1 pyramidal cells, appears to be a high-voltage-activated R-type channel, multiple R-type channels with different activation and inactivation characteristics have been identified (Tottene et al., 1996, 2000; Sochivko et al., 2002). Third, models should include calcium release from stores when spines are mushroom-shaped and probably should at least consider release from stores in non-mushroom-shaped spines.

3.6.2 Calcium Extrusion via Pumps

Work has been done to identify calcium extrusion mechanisms and their effectiveness in reducing the calcium transient. This work is difficult because fluorescent indicators buffer calcium and distort estimates of the extrusion time course. Furthermore it is difficult to separate calcium transient decay due to buffers or diffusion from decay due solely to pumps. The contribution of buffers, pumps, and diffusion to the decay of the calcium transient will be different in different shaped spines.

It is generally assumed that there are three types of pumps in spines: the SERCA pumps that pump calcium into calcium stores (SER), the plasma membrane calcium ATP pump (PMCA, Guerini and Carafoli, 1999), and the $\text{Na}^+-\text{Ca}^{2+}$ exchanger (Philipson, 1999). Sabatini et al. (2002) estimated that about 30% of the calcium clearance from spines was due to SERCA pumps, although results were highly variable from spine to spine, perhaps because of the presence or absence of an SER in different spines (Spacek and Harris, 1997). They concluded that the other 70% must be due to the PMCA pump and the $\text{Na}^+-\text{Ca}^{2+}$ exchanger. Blocking the SERCA pumps slowed the decay time constant of the transient by 50% (Sabatini et al., 2002) or over 100% (Majewska et al., 2000a). In addition, Majewska et al. (2000a) observed a 35% increase in the fluorescence signal when SERCA pumps were blocked, presumably because more calcium was available. Holthoff et al. (2002) found that calcium clearance scales linearly with surface area, which would be consistent with a role for plasma-membrane pumps.

When the effects of the exogenous buffer (the indicator) and temperature are taken into account in these studies of calcium clearance from spines, what is remarkable about the results is how fast extrusion mechanisms clear calcium. Majewska et al. (2000a), Sabatini et al. (2002), and Holthoff et al. (2002) all agree that without the dye, the clearance time constant is 10 to 20 msec. It should be noted that this time constant combines the effects of buffered diffusion and extrusion, which will vary from spine to spine. Given the relatively slow turnover rate of a single pump, these data imply that pump density must be extremely high or that estimates of pump turnover rate are very low (perhaps because temperature was not physiological). The three studies also agree that endogenous buffers and pumps are not saturated, since the decay time constant appears to be the same whether calcium transients are elicited once or several times at high frequency (Sabatini et al., 2002).

3.6.3 Calcium Buffers in Spines

The number, types, concentrations, and kinetics of calcium buffers in dendritic spines are still largely unknown. However, recent experimental work has revealed some characteristics of the calcium buffer in spines. Endogenous buffer capacity in spines has been estimated to be about 20 (Sabatini et al., 2002). This means that 95% of the calcium entering the spine is buffered, with 5% remaining free. This is in contrast to higher estimates of buffer capacity in CA1 pyramidal-cell dendrites which are 60 to 200 (Helmchen et al., 1996; Lee et al., 2000; Murthy et al., 2000).

Another question of interest to modelers is whether the calcium buffer is mobile or not. Cerebellar Purkinje cells have a large concentration of a mobile high-affinity buffer, thought to be calbindin (Maeda et al., 1999), along with an immobile low-affinity buffer. In contrast, the calcium buffer in CA1 pyramidal cells appears to be slowly mobile or immobile. In these cells the calcium buffer does not seem to wash out during whole cell recordings as might be expected if it were mobile, suggesting that mobile buffers do not contribute significantly to calcium buffering in spines (Sabatini et al., 2002). Murthy et al. (2000) estimate the diffusion constant for the calcium buffer to be 10 to 50 $\mu\text{m}^2 \text{sec}^{-1}$ or an order of magnitude slower than the calcium diffusion coefficient (223 $\mu\text{m}^2 \text{sec}^{-1}$, Allbritton et al., 1992). Many models use calmodulin as the major calcium buffer, but can calmodulin be considered to be an immobile buffer? Calmodulin, based strictly on size, would be expected to diffuse about an order of magnitude slower than calcium. At resting calcium levels calmodulin may be bound to neurogranin, but with calcium influx, calmodulin may be released allowing it to bind to calcium-calmodulin dependent protein kinase II (CaMKII) or calcineurin. Given that calmodulin itself may be “buffered” both at rest and during activity, calmodulin seems to have the necessary properties to be a major buffer of calcium in spines.

Finally experimental work suggests that, whatever the calcium buffer may be in spines, it is not saturated by strong input (Sabatini et al., 2002). If calmodulin were the only calcium buffer and if calmodulin concentration in spines were about 40 μM , then calmodulin itself would be capable of binding up to 160 μM of calcium. Given the size of observed calcium transients and the buffer capacity estimates for spines, it would seem that calmodulin can be a major, but not the only, calcium buffer in spines. This point is explored further in the problems presented at the end of the chapter.

3.7 ADDITIONAL INSIGHTS INTO SPINE FUNCTION FROM EXPERIMENTAL STUDIES

There have been a number of new insights into spine function from experimental work beyond insights into calcium dynamics. Here I shall focus on just two: spine motility and coincidence detection with backpropagating action potentials.

3.7.1 Spine Motility

Actin filaments are highly concentrated in spines and it was this high concentration of actin that led Crick to propose that calcium entry into spines might cause them to “twitch” in a way analogous to how calcium causes muscle contraction (Crick, 1982). The use of imaging techniques has allowed investigators to monitor spines in real time and it has been found that while some spines remain stable for hours or days, others are constantly changing shape over periods of seconds (Fischer et al., 1998). The highest levels of spine motility are observed in periods of development when synaptogenesis occurs (Dunaevsky et al., 1999). Spine shape tends to become more stable with age and synaptic activation, as more of the dynamic actin is replaced by stable actin. Nevertheless, spine motility has been observed at mature synapses. Morphological changes observed in development and following severe or traumatic events in the adult are dependent on activity-induced spine calcium levels. When there is a lack of activity and spine calcium levels are low, there may be a transient outgrowth of spines, but if calcium remains low, the spine may retract and be eliminated. Moderate increases of spine calcium promote spine elongation, but high levels may cause shrinkage and retraction (Segal, 2001). Such changes can occur in the normal adult, but usually they are much less pronounced.

What are the implications of spine motility for spine function? First, spine motility suggests that synaptic weights at spines are constantly changing. These changes could be subtle or significant. Shape changes can produce small electrical effects, but can also affect the amplitude and decay-time constant of the calcium transient significantly, leading to changes in calcium-initiated reaction cascades (Majewska et al., 2000a; Bonhoeffer and Yuste, 2002; Holzman et al., 2004).

Any increase or decrease in spine size may permit or be accompanied by a change in the number of postsynaptic receptors. Second, actin-based motility may position macromolecular complexes in a signal-dependent manner (Halpain, 2000). Numerous proteins make up the structure of the postsynaptic density (PSD) and how these are arranged at the synapse may depend in part on how and when they are tethered to or released from actin. Even low levels of motility could conceivably produce significant rearrangements of PSD proteins. Third, spine motility may help stabilize or destabilize the connections between the pre- and postsynaptic sides of the synapse. As the spine pushes out or retracts, the relationship between the sites of vesicle release and locations of postsynaptic receptors is tested.

3.7.2 Coincidence Detection with Backpropagating Action Potentials

Experiments in both neocortex and CA1 hippocampus have shown that pairing one or more EPSPs with a backpropagating action potential produces a supralinear summation of the calcium signals seen with either stimulus alone (Koester and Sakmann, 1998; Yuste et al., 1999). Summation was supralinear when the EPSPs preceded the action potential within a short time interval, but was sublinear with the reverse pairing. The supralinear summation is thought to occur because the backpropagating action potential relieves magnesium block of NMDA-receptor channels, allowing more calcium to enter. With the reverse pairing, the depolarization due to the action potential is largely over when the NMDA receptors are activated and no relief of magnesium block occurs. The spine “detects” the coincident pre- and postsynaptic activation by producing a larger calcium transient, but this detection only occurs when the signals are in the proper order.

Models in which spines have NMDA-receptor channels but not voltage-gated calcium channels show a notch in the spine calcium transient at the time when the action potential propagates back to the spine, and how much actual boosting of the calcium signal occurs depends on the width of the action potential (cf. figure 3A, Holmes, 2000). In most cases this boosting of the calcium signal is modest. NMDA-receptor channels are blocked very quickly by magnesium, so any relief of the magnesium block would only last as long as the action potential. To explain the supralinear summation observed experimentally, models need to incorporate appropriate types and numbers of voltage-gated calcium channels as well as NMDA-receptor channels at spines. It is possible that the relief of the magnesium block that occurs when the action potential backpropagates to the spine may be enough to cause a voltage boost sufficient to provide additional activation of voltage-gated calcium channels and, in a regenerative manner, additional NMDA-receptor channel activation, but this remains to be tested.

3.8 SECOND-GENERATION SPINE MODELS: REACTIONS LEADING TO CaMKII ACTIVATION

While first-generation spine models searched for a nonlinearity in spine-head calcium concentration as a function of input frequency and strength, second-generation models search for this nonlinearity in CaMKII activation. Much work suggests that strong calcium signals may induce LTP by activating CaMKII (for reviews see Soderling, 1993; Lisman, 1994; Fukunaga et al., 1996; Lisman et al., 1997). When calcium enters the spine, it binds to calmodulin and the calcium-calmodulin complex (CaM Ca_4) can then bind to individual subunits of CaMKII and activate them. Activated subunits can react with ATP to add a phosphate group at one or more positions in the subunit in a process called autophosphorylation, and this can allow the subunit to remain activated even when CaM Ca_4 is no longer present. Second-generation models have sought to determine the stimulation conditions that lead to significant CaMKII activation, the time course of CaMKII activation, and the possible role of spine shape in CaMKII activation.

3.8.1 Modeling CaMKII Activation is Complicated

A CaMKII holoenzyme consists of two rings composed of six subunits each. Each subunit can be activated independently by CaM Ca_4 . A subunit activated by CaM Ca_4 binding (the *bound* state) can be phosphorylated at the T²⁸⁶ position (here we consider only the α subunit type), but only if its immediate neighboring subunit in the ring is also activated. It is not clear whether this intersubunit autophosphorylation can occur only in the clockwise direction, in the counterclockwise direction, or in both directions. Once a subunit is phosphorylated at T²⁸⁶, the rate of CaM Ca_4 dissociation from CaMKII is extended from tens of milliseconds to tens of seconds. We say that CaM Ca_4 is *trapped* on the subunit or that the subunit is in the trapped state, following the notation of Hanson and Schulman (1992). Eventually CaM Ca_4 unbinds and the subunit, still phosphorylated at T²⁸⁶, is considered *autonomous*. The subunit is still activated, but it does not require calcium to remain activated. Once CaM Ca_4 unbinds, the calmodulin binding site in an autonomous subunit can be rapidly autophosphorylated at positions T^{305,306} and the subunit is considered to be *capped*. This capping reaction may be either an intrasubunit or intersubunit autophosphorylation, although the experimental evidence is sparse for either case. The belief that the reaction is intrasubunit stems from the evidence that the slow basal autophosphorylation at T³⁰⁶ alone (to the *inhibited* state) is intrasubunit (Mukherji and Soderling, 1994); with phosphorylation at T²⁸⁶ it is thought that conformational shifts will allow both T³⁰⁵ and T³⁰⁶ to be in a better position for intrasubunit autophosphorylation. The belief that the capping reaction is intersubunit (dependent on the activation state of an immediately neighboring subunit) is based on a footnote in Mukherji and Soderling (1994) saying that they found evidence for this belief. This evidence remains unpublished.

It is thought that the bound and trapped states represent higher activity states than the autonomous and capped states. In fact the capped state is sometimes called an inhibited state because it cannot be brought back to the more highly activated bound and trapped states by calcium signals until it is dephosphorylated at T^{305,306}. Strictly speaking, the term “inhibited” should be reserved for the small number of subunits that spontaneously undergo basal autophosphorylation at the T³⁰⁶ site. Figure 3.2 shows kinetic reactions starting with calcium binding to calmodulin and calcium-calmodulin binding to CaMKII and calcineurin followed by transitions of activated CaMKII through the trapped, autonomous, and capped states. We have omitted the inhibited state from this figure because the reaction producing this state is slow and is likely to be reversed by phosphatase activity.

The time course of CaMKII activation will depend on the dephosphorylation action of phosphatases. Protein phosphatases 1 and 2A (PP1 and PP2A) are thought to dephosphorylate CaMKII but in different locations. PP2A dephosphorylates CaMKII primarily in the cytoplasm whereas PP1 primarily dephosphorylates CaMKII that has translocated to the postsynaptic density (Strack et al., 1997a, 1997b). PP1 activation is controlled by Inhibitor-1 which, when phosphorylated by PKA, inactivates PP1. Inhibitor-1 is dephosphorylated by calcineurin (PP2B), which is activated by CaM Ca_4 . Thus, phosphatase activity is also tightly regulated, leading many to postulate that the balance between CaMKII phosphorylation and dephosphorylation determines whether LTP is induced or not.

3.8.2 Characteristics of Second-Generation Models

Second-generation models differ in their modeling approach (deterministic or stochastic), whether or not the calcium signal is arbitrary, and whether phosphatase dynamics is included. Unfortunately, very few of these models actually consider CaMKII activation and phosphatase dynamics in the context of a dendritic spine. Those that do begin with the equations outlined earlier in Section 3.2, let calmodulin be the primary calcium buffer, and add equations for CaMKII and phosphatase dynamics as described below. If calmodulin, CaMKII, or phosphatase is allowed to diffuse, then equations analogous to Equation (3.1) are also needed for these substances.

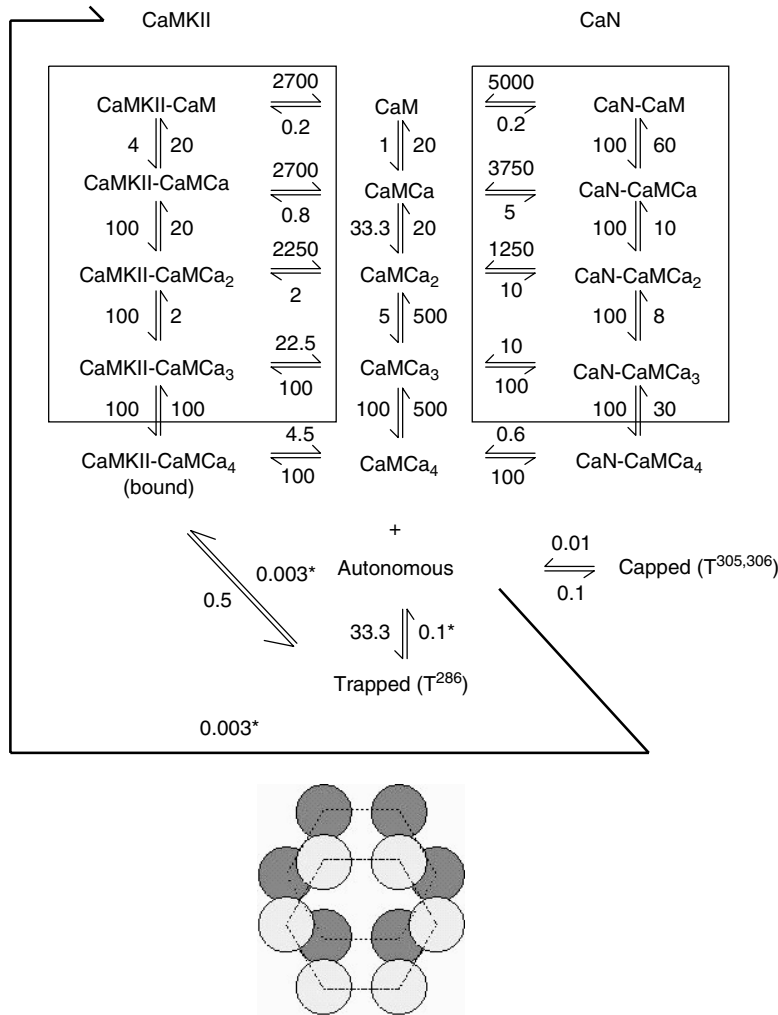


FIGURE 3.2 A summary of the reactions leading to CaMKII activation. Rate constants are those used in Holmes (2000). Units are $\mu\text{M}^{-1}\text{sec}^{-1}$ and sec^{-1} . Calcium binds to calmodulin as shown in the middle. Calmodulin with 0, 1, 2, 3, or 4 calcium ions bound binds to CaMKII or calcineurin (CaN). CaMKII with CaMCA₄ is considered to be in the bound state. A bound subunit may be autophosphorylated to become trapped. If CaMCA₄ unbinds from a trapped subunit, it becomes autonomous. An autonomous subunit can rebind CaMCA₄ to become trapped again. An autonomous subunit can be autophosphorylated at the calmodulin binding site to become capped. In the illustrated scheme, a capped subunit must be dephosphorylated back to the autonomous state and the autonomous state can be dephosphorylated to return the subunit to the free state. At the bottom is a cartoon of two rings of six subunits each meant to represent a CaMKII holoenzyme.

3.8.2.1 Deterministic vs. Stochastic

Models by Coomber (1998a, 1998b), Kubota and Bower (2001), Zhabotinsky (2000), and Okamoto and Ichikawa (2000a, 2000b) use differential equations to model calcium binding to calmodulin and the CaMKII activation reactions shown in Figure 3.2. Because each subunit can be in 12 different states with each holoenzyme having 8 to 10 subunits in Coomber's model, each enzyme can have 8^{12} to 10^{12} configurations. To reduce the number of equations, Coomber (1998a, 1998b) considers only four or five subunits per holoenzyme and combines states that are similar, reducing the number of equations to about 3000. Kubota and Bower (2001) also limit the number of subunits per holoenzyme

to four to reduce the computational load. In contrast, Michelson and Schulman (1994) and Holmes (2000) model the CaMKII activation reactions stochastically (reactions in the lower part of Figure 3.2). This approach involves much bookkeeping. When CaM Ca_4 binds to a CaMKII subunit, the particular holoenzyme and the particular subunit on that holoenzyme where binding occurs are assigned randomly. This is necessary because of the dependence of subsequent autophosphorylation reactions on the state of neighboring subunits. Similarly, at each time step, random numbers are chosen for each bound, trapped, autonomous, and capped subunit to determine which subunits make transitions to which neighboring states.

3.8.2.2 Calcium Signal

Second-generation models also differ with respect to the calcium signal used. Because models are interested in CaMKII dynamics and/or phosphatase dynamics, and, as we have seen above, the calcium signal in dendritic spines can be quite variable, depending on many factors, most models assume a simple form for the calcium transient. This form ranges from constant calcium concentration or regular calcium oscillations (Okamoto and Ichikawa, 2000a, 2000b), to calcium pulses (Dosemeci and Albers, 1996; Kubota and Bower, 2001; d'Alcantara et al., 2003), to step increases in calcium with exponential decay (Zhabotinsky, 2000), to exponential rise and exponential decay (Coomber, 1998a, 1998b), and to calcium influx through NMDA-receptor channels computed at a spine in a neuron-level model (Holmes, 2000) with NMDA-receptor channel openings computed either deterministically or stochastically with a synapse-level model. The use of simple calcium signals reduces computational demands of the simulations and allows insights to be obtained about what might be happening in spines, but at some point it will be necessary to model these processes within the context of actual dendritic spines to distinguish what is feasible in a model from what happens physiologically.

3.8.2.3 Calcium Binding to Calmodulin

Given the calcium signal, the next step is to model calcium binding to calmodulin. Calmodulin can bind four calcium ions, two on the N-lobe and two on the C-lobe. The binding is cooperative within a lobe. What is important for the models is that the affinity of CaMKII and calcineurin for calmodulin is very low until at least three and usually four calcium ions bind to calmodulin. Once calmodulin binds to CaMKII or calcineurin, the affinity of calmodulin for calcium increases significantly, particularly at the low-affinity binding sites. These experimental observations are built into the sample rate constants illustrated in the kinetic scheme of Figure 3.2. Consequently, the calmodulin state of primary interest for models is CaM Ca_4 .

How models compute the concentration of CaM Ca_4 varies. Coomber (1998a), Okamoto and Ichikawa (2000a, 2000b), Zhabotinsky (2000), and d'Alcantara et al. (2003) use either a simple binding scheme where all four calcium ions bind at once or a version of the Hill equation. Kubota and Bower (2001) use an Adair-Klotz equation formulation (equation shown in Table 3.2), while Holmes (2000) uses the elaborate sequential binding scheme shown in Figure 3.2. Parameter values used in various models are given in Table 3.2. Because different investigators use different procedures to calculate CaM Ca_4 , we will not present specific differential equations here. The reader is advised to examine the individual references mentioned for specific details. However, it is straightforward to translate biochemical reactions, such as those shown in Figure 3.2, into differential equations and some examples that can be applied to calcium binding to calmodulin are given in Appendix 1.

3.8.2.4 CaMKII Autophosphorylation Reactions

Once calcium has bound to calmodulin to produce CaM Ca_4 , CaM Ca_4 can bind to and activate CaMKII, creating a bound subunit. Although the affinity of CaMKII for CaM Ca_4 seems quite high

